Onset of Flow Reversal and Penetration Length of Natural Convective Flow Between Isothermal Vertical Walls

K. D. Kihm,[1,4] J. H. Kim,[2,4] and L. S. Fletcher[3,4]

Nomenclature

b = channel half-spacing
H = channel depth
L = channel height
L_p = penetration length of flow reversal
Nu_b = average Nusselt number based on b
Pr = Prandtl number
R = radius of extended upstream region from the channel entrance
Ra_b = Rayleigh number = $Gr_b \cdot Pr$
Ra^* = modified Rayleigh number = $Ra_b \cdot (b/L)$
x, y = coordinate system for physical geometry

[1]Associate Professor; Mem. ASME.
[2]Presently at Korea Aerospace Research Institute. Taejon, Korea.
[3]Thomas A. Dietz Professor; Fellow ASME.
[4]Department of Mechanical Engineering, Texas A&M University, College Station, TX 77843-3123.

Contributed by the Heat Transfer Division of THE AMERICAN Soctm of MECHANICAL ENGINEERS. Manuscript received by the Heat Transfer Division October 1994; revision received December 1994. Keywords: Flow Visualization, Natural Convection, Numerical Methods. Associate Technical Editor: R. Viskenta.

Introduction

Thermally driven flows in a vertical heated channel form a basic structure for various heat transfer devices. Typical applications include electronic packaging systems and heat exchangers. Heat transfer characteristics of the flow to and from the channel walls have been studied extensively, with many studies of channel flows available. The onset and penetration lengths of the flow reversals, however, have received only limited attention. The present study of flow reversals occurring in vertical isothermal channels uses a convenient numerical technique with experimental substantiation by means of smoke visualization.

Since the pioneering work of convective heat transfer phenomena in heated vertical channels conducted by Elenbaas (1942), there have been a number of relevant investigations using various analytical, numerical, and experimental techniques. Eckert et al. (1990) presented an extensive review of publications dealing with natural convection in vertical channel flows. Many different aspects of the problem have been identified and investigated, including local and average correlations of heat transfer coefficients, isotherms, and streamlines for narrow or wide channel flows, symmetrically or asymmetrically heated channels, vertical and inclined arrangements and, more recently, parallel and converging channels (Kihm et al., 1993). These aspects have been studied for forced, mixed, and natural convection problems. There are more studies for forced or mixed convection primarily because of their relative simplicity arising from the parabolic nature of the problems. Natural convection problems, however, are generally more cumbersome because of the nontrivial contribution of transverse and axial diffusion effects, i.e., the elliptic nature of the problem.

Sparrow et al. (1984) investigated the flow reversal by visualizing water flows (Pr = 5.0) in a vertical channel heated on one side. They showed that a single dimensionless group, $Ra_b \cdot (2b/L)$, where $2b$ represents the channel spacing and L is the channel height, correlated their Nusselt number results well. Chang and Lin (1990) presented a numerical simulation of the transient process of flow reversal in a vertical channel with one side heated. They observed that the velocity and temperature wakes above the heated plate were oscillatory when Rab was larger than 10^6. Naylor et al. (1991) introduced Jeffrey-Hamel flow for the far-field inlet boundary conditions in their numerical study of flow between isothermal walls. Their elliptic solution identified a flow separation near the chapnel inlet where the Rayleigh number exceeded a critical value, which resulted in a minimal local Nusselt number. As the study focused on the channel inlet region, the flow reversal occurring near the channel exit was not discussed.

The present paper identifies the occurrence of the onset and penetration lengths of the flow reversal in natural convection flow through vertical isothermal channel walls in terms of the modified Rayleigh number $Ra^* = Ra_b \cdot (b/L)$ and the channel aspect ratio L/b (Fig. I).

Analytical and Numerical Study

The standard elliptic forms of the steady two-dimensional mass, momentum, and energy equations were solved using a finite difference method with a body or boundary-fitted coordinate transformation (BFCT). A comprehensive description of general BFCT technique is given by Thompson et al. (1974) and a detailed description of the scheme applied to the present problem is presented by Kim (1993) . Laminar flow was assumed with a Boussinesq approximation. The thermal boundary conditions are isothermal at the vertical walls, adiabatic at the ceiling of the extended semicircle, and zero gradient at the extended inlet and channel exit. The boundary conditions imposed for the velocity field are no-slip on all solid surfaces, including the ceiling, with Neumann conditions at the inlet and exit.

The half-domain of symmetry consisted of a total of 4961 graded grids with a 3 percent average expansion or contraction grading. The radius of the extended region, R, was equal to ten times the channel half-spacing, b, as preliminary calculations with a setting $R = 10b$ converged within 2 percent of those with a larger radius of $R = 20b$. The BFCT technique successfully transformed a unique configuration consisting of the channel and the semicircular extended upstream inlet into a rectangular domain on which the numerical analysis was carried out. The dimensionless stream function, vorticity, and temperature were integrated using iterations by successive overrelaxation (SOR) with convergence of 10^{-6} or less until the mass continuity was satisfied.

The onset of flow reversal was the value of Ra* that first resulted in a negative streamline detached from the centerline. Pocketlike streamlines with negative constants represented the formation of a recirculating flow. The recirculating flow penetrates into the channel along the centerline or zero streamline, splits into two separate flows at the stagnation point and then each flow merges into the upcoming flow along the channel wall. The maximum penetration length is the distance from the channel exit to the stagnation point on the centerline.

Calculations were made for air, Pr = 0.7, a modified Rayleigh number range of 0.05 < Ra* < 2000, and channel aspect ratios of L/b = 2, 5, 8, 10, and 24. The calculated heat transfer coefficients showed excellent agreement with previous data (Kim, 1993). The average Nusselt number, Nu_b, correlated well with the modified Rayleigh number Ra* = Ra_b.(b/L).

Flow Visualization Study

An experimental test facility for the flow visualization of recirculating flow behavior in isothermal vertical channels was developed. Each of the vertical isothermal walls was made of 0.826-cm-thick aluminum plate with a vertical length, L, of 12.7 cm and a depth, H, of 20.32 cm. Each plate had a heater pad attached to the backside with a total of nine K-type thermo couples embedded within 1 mm depth from the front surface. When steady-state conditions were reached, the maximum discrepancies between the thermocouple readings were ±0.4°C for the lowest Ra* that required the heated plate temperature only a few degrees higher than the ambient temperature. The channel sides were covered with 3-mm-thick glass plates to reduce the edge effect. To ensure the no-slip condition at the ceiling (y = 0), as specified in the numerical analysis, a Plexiglas panel was placed next to the leading edge of each isothermal plate.

A Rosco Fog machine generated smoke based on the method of nucleus condensation. The smoke passed through several regulation stages to ensure minimal flow momentum near the channel inlet. The chamber contained two guide vanes to reduce and diffuse the smoke flux from the generator and to cool the smoke to the ambient level. 4 × 4 mesh screens (6.35 mm mesh dimension) were installed at both the inlet and exit of the duct to reduce the flow disturbance. A deflector was placed at the duct exit to reduce the directional movement of the smoke flow, which would not be desirable for the flow visualization study. Finally, in order to ensure uniformly distributed smoke flow to the test channel, another fine mesh screen (3.18 mm mesh dimension) was placed at the channel entrance.

The smoke temperature was measured just before the channel entrance and maximum deviations were 1.3°C higher than the ambient temperature. The residual smoke, which was not introduced into the test section, was allowed to diffuse freely into the laboratory. A 35-mm camera, with 1 /250 second exposure time, recorded the smoke flow patterns under fluorescent lighting boosted with a strobe flash. A ruler attached to the heated wall measured the penetration lengths.

The length of the recirculating flow was persistent and reasonably stable for the period of observation. The measurement uncertainties associated with the reading errors were estimated to be one medium division of the ruler, i.e., ±2.5 mm, as a very conservative estimation, or less than ±3 percent. The measurement uncertainties of the wall temperature were estimated as a maximum of ±0.3 percent, and the resultant uncertainties in the Rayleigh number were estimated as ± 1 percent. Thus, the overall uncertainties involved in measuring the flow reversal lengths were estimated to be less than ±5 percent. An attempt to determine the onset condition experimentally for flow reversal was not successful, since the physical uncertainties of the flow near the onset condition were too high to identify the critical Rayleigh number with acceptable accuracy.

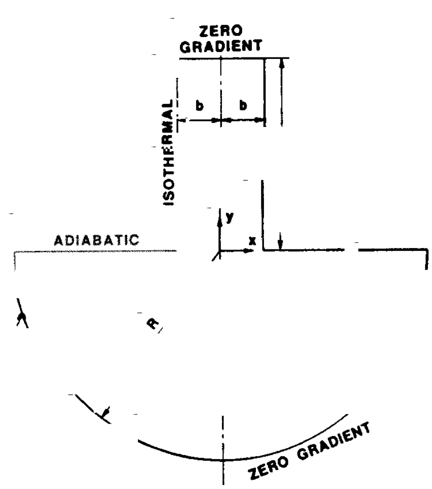

Fig. 1 The computational domain for convective air flow in vertical isothermal channel configuration

Results and Discussion

Figures 2(a, b, c) show the numerically calculated streamlines (left side) and isotherms (right side) for Ra * = 1, 100, and 500 for the case of $L/b = 8$, respectively. The inset photographs were taken from the smoke visualization experiment of the flow stream at Ra * = 130.2 and 501.8. The extended inlet regions are shown only up to twice the channel half-spacing. The dimensionless isotherms have a value of one at the isothermal wall and zero at free stream and infinity. The dimensionless stream line takes a value of zero at the centerline. For the case of Ra* = 1 (Fig. 2a), the almost uniform intervals between streamlines show that the flow is fully developed. The weak air flow induced by the low thermal driving force allows the isotherms to extend well into the upstream entrance region due to the elliptic nature of the relatively strong conduction effect. As a result, the incoming air is preheated and the temperature at the channel inlet can be as much as 30 percent higher than the ambient or far-field inlet temperature. Thus, a parabolic simplification assuming uniform inlet temperature would cause a significant error for such low Rayleigh number cases.

The flow field at Ra * = 100 (Fig. 2b) deviated from the previous fully developed case and the depleted streamlines near the channel center show separate boundary layer development.

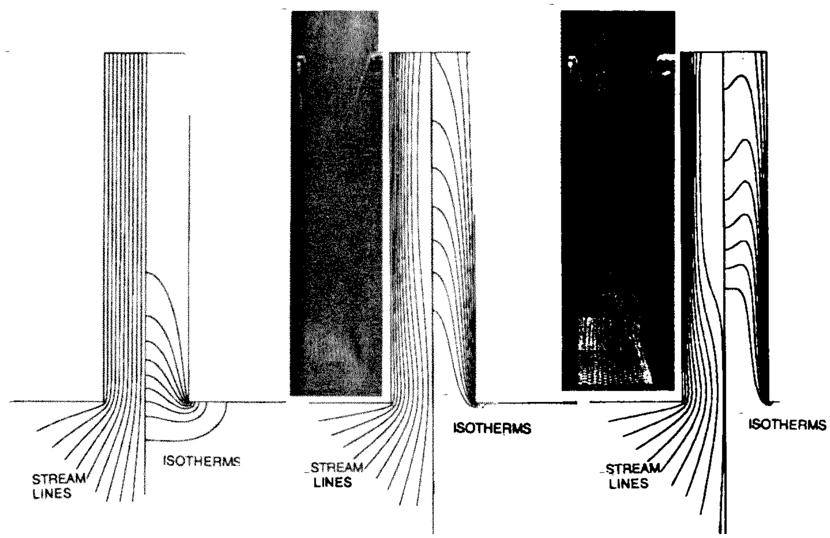

(a) Ra^* = 1.0 (b) Ra^* = 10 (c) Ra^* = 500

Fig. 2 Calculated flow streamlines and isotherms of convective air (Pr = 0.7) for *L/b = 8:* (a) Ra* = 1.0; (b) Re* = 100; and (c) Re* = 500. The photographs indicate smoke stream visualization at Ra* = 130.2 and *501.8,* respectively.

The more concentrated streamlines appearing near the wall suggest increased buoyancy-driven air flow. Also, this increased convection reduces the penetration of the conduction effect at the inlet as seen in the isotherm distributions.

Figure 2 (c) shows the streamlines and isotherms when Ra* is increased to 500, which exceeds the critical Rayleigh number (Ra* = 146 as numerically determined). The congested streamlines near the wall indicate that most induced air flow concentrates in the narrower boundary layer next to the wall. The pocketlike streamlines appear with negative constants demonstrating the formation of recirculating flow. Vena-contracts-like streamlines at the entrance appear to reduce the effective opening. This narrower effective opening reduces the incoming air, whereas the increased thermal driving force requires more air flow. When the acceleration of the air flow near the channel wall exceeds a critical point, the incoming air flow through the inlet is insufficient and additional air drawn in through the central portion of the channel exit results in flow reversal. The

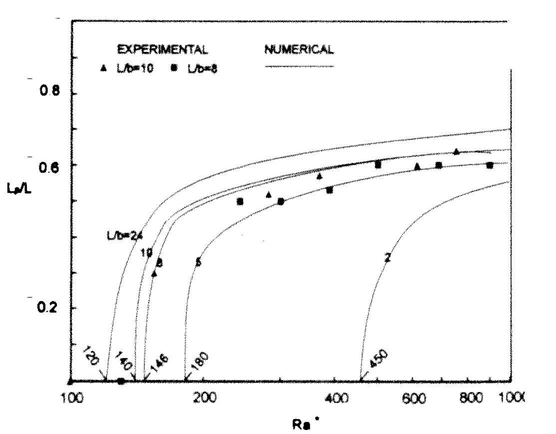

Fig. 3 Experimental and numerical results of the penetration length versus Re ' and numerically predicted onset Rayleigh numbers for flow reversal

isotherms show that the temperature in the recirculation region is significantly lower than the air temperature next to the wall at the same y position. This indicates that the convection heat transfer to the recirculating air from the wall is limited and the overall heat transfer is not significantly altered by the presence of the flow reversal. The fact that the conduction preheating of the incoming air, or the elliptic nature of the problem, has noticeably been reduced with the occurrence of flow reversal, implies that the channel flow problem can be approximated with a parabolic simplification when Ra* exceeds the critical value for the flow reversal.

Figure 3 shows that the calculated onset Rayleigh numbers that initiate the flow reversals are 120, 140, 146, 180, and 450, respectively, for L/b = 24, 10, 8, 5, and 2. The numerically and experimentally observed penetration lengths of the channel flows are also provided in Fig. 3. Although the present experimental configuration allowed only two channel aspect ratios, 8 and 10, the data favorably supported the numerical results. Ra_b is the flow parameter that determines the level of natural convection strength and L/b is the geometric parameter. It appears that the penetration length increases for increasing channel aspect ratio, L/b, for the same Ra* = Ra_b·(b/L). This is primarily because of higher flow parameter Rab required to keep Ra constant as the channel is longer with smaller b/L. This higher Ra_b also explains the fact that the onset of the flow reversal for longer channel occurs earlier at relatively smaller Ra*. Another thing to note here is that the deviation observed between the data and predictions particularly in lower Ra* range is probably attributed to the simplified free boundary condition imposed at the channel exit. For further investigation of the problem, a downstream extended region with a far-field free boundary condition needs to be considered to incorporate the possible elliptic behavior at the channel exit.

References

Chang. T. S., and Lin. T. F., 1990, "On the Reversed Flow and Oscillating Wake in an Asymmetrically Heated Channel," ***/nternational Journal for Numerical Methods in Fluids,*** Vol. 10, pp. 443-459.

Eckert, E. R. G., Goldstein. R. J., Irvine, T. F., and Hartnett, J. P.. 1990, ***Heat Transfer Reviews 1976-1986,*** Wiley. New York.

Elenbaas, W., 1942, "Heat Dissipation of Parallel Plates by Free Convection," Physica, Vol. 9, pp. 1-28.

Kihm, K. D., Kim, J. H., and Fletcher, L. S., 1993, "Investigation of Natural Convection Heat Transfer in Converging Channel Flows Using a Specklegram Technique," ASME JOURNAL OF HEAT TRANSFER, Vol. 115, No. 1, pp. 140-148.

Kim, J. H., 1993, "Investigation of Heat Transfer Characteristics and FlowReversal Phenomena in Natural Convecting Parallel / Converging Vertical Channel Flows." Ph.D. Thesis, Department of Mechanical Engineering, Texas A&M University.

Naylor, D., Floryan. J. M., and Tarasuk. J. D., 1991, "A Numerical Study of Developing Free Convection Between Isothermal Vertical Plates," ASME Journal of Heat Transfer, Vol. 113, pp. 620-626.

Sparrow, E. M., Chrysler, G. M., and Azevedo, L. F., 1984, .'Observed Flow Reversals and Measured-Predicted Nusselt Numbers for Natural Convection in a One-Sided Heated Vertical Channel," ASME Journal of Heat Transfer, Vol. 106, pp. 325-332.

Thompson, J. F., Thames, F. C., and Mastin, C. W., 1974, "Automatic Numerical Generation of Body-Fitted Curvilinear Coordinate System for Field Containing Any Number of Arbitrary Two-Dimensional Bodies," Journal of Computational Physics, Vol. 15, pp. 299-319.